Bull. Astr. Soc. India (1988) 16, 93–110

Ooty synthesis radio telescope : design and performance

S. Sukumar, T. Velusamy, A. Pramesh Rao, G. Swarup, D. S. Bagri, M. N. Joshi & S. Ananthakrishnan

Radio Astronomy Centre, Tata Institute of Fundamental Research, Post Box 8, Udhagamandalam 643 001

Received 1988 February 29; accepted 1988 April 10

Abstract. The principle, design, and operational parameters of the Ooty synthesis radio telescope (OSRT) are described. It consists of thirteen elements including the Ooty Radio Telescope which is divided into five parts. Operating at 327 MHz OSRT provides a resolution of about 36 × 60 arcsec² and a sensitivity of about 4 mJy for 9 hour observation.

Key words : radio astronomy—aperture synthesis—instrumentation—image processing

1. Introduction

The technique of aperture synthesis radio telescopes was first developed by Ryle (1962) at Cambridge and several synthesis telescopes have since been constructed in different parts of the world. Notable among these are the very large array (VLA) in the USA; Westerbork synthesis radio telescope (WSRT) in The Netherlands; Molonglo synthesis radio telescope (MOST) in Australia; and the multi element radio link interferometer (MERLIN) in England. The system parameters of some of these telescopes operating at 20cm and longer wavelengths are given in table 1. Most of these telescopes operate at shorter wavelengths and are situated at higher latitudes while the recently completed Ooty synthesis radio telescope (OSRT) in India has been designed to fill the need for a synthesis radio telescope operating at meter wavelengths covering both the northern and the southern sky.

The brief description of OSRT and the preliminary results obtained are given in Swarup (1984). The dipole array of the parabolic cylindrical antennas of OSRT is described by Joshi *et al.* (1988), the receiver system by Narayana *et al.* (1988), and the antenna control system by Sankararaman *et al.* (1982). In this paper we describe the operational characteristics of OSRT, emphasizing the system capabilities to achieve high resolution over large fields of view ranging from 3°.0 × 0°.7

Table 1. Synthesis radio telescopes operating at meter and cm wavelengths

Name	Frequency (GHz)	No. of elements	Total Geo-metrical area (m^2)	Array size (km) and geometry	Resolution at lowest frequency (arcsec)
Cambridge	0.151	60 × 4 element Yagis	2000	5 0 E/W	82
Fleurs, FST	1.4	64 × 6m dish 6 × 14m dish	2700	1.6 E/W, 0.8 N/S 3.6 Irregular	12
Gauribidanur Decameter Wave Telescope	0.035	1000 dipoles	60000	1.4 E/W 0.45 N/S	1560
MERLIN	0.408, 1.66 5.0, 22	1 × 76m dish 2 × 15m dish 3 × 25m dish	6362	134 Irregular	1.1
Molonglo Obs. Synthesis Telescope	0.843	2 nos. 778m × 11.6m	18068	1.6 E/W	43
Ooty synthesis Radio Telescope	0.327	5 × 30m × 92m cyl. 7 × 9m × 23m cyl.	15250	2.1 N/S 4.2 E/W	36
Pentiction, DRAO	0.408, 1.4	4 × 9 dish	254	0.6 E/W	252
Socorro, VLA	0.327, 1.4 5, 14.4, 23	27 × 25m dish	13200	36 Y	5
Westerbork, WSRT	0.327, 0.608, 1.4, 5.0	14 × 25m dish	6872	2.8 E/W	67

to 3°.0 × 2°.0. We also briefly outline the principle of aperture synthesis, array configuration and the design of OSRT.

2. Principle of aperture synthesis

The principle of radio interferometers synthesizing large apertures by correlating the voltages received at the antenna elements has been extensively described in the literature (*e.g.* Bracewell 1958, Swenson & Mathur 1968). Recent reviews on aperture systhesis and imaging are given in the 1985 *NARO summer school on Synthesis imaging* (eds : A. Perley, F. R. Schwab & A. H. Bridle). A radio interferometer in which the voltages received by two elements are correlated measures the amplitude and phase of the Fourier component of the sky brightness distribution, corresponding to the separation **b** between the antennas. With an interferometer having many elements, it is possible to measure simultaneously several Fourier components of the sky brightness distribution corresponding to the different baselines between the antennas. The correlator, which multiplies the signals from different antenna pairs and integrates over a pre-determined time, produces an output having quasisinusoidal fringes. The quasisinusoidal fringes have an angular separation (λ/b cycles per radian) where b is the projected spacing of the antennas as seen

by the source and λ is the wavelength. Thus amplitude and phase of these fringes, when properly calibrated, represent the complex visibility of the brightness distribution measured at the spatial frequencies corresponding to the fringe separation. The complex visibility V is related to the brightness distribution B by a simple Fourier transform relationship given by

$$V(\mathbf{s}) = \int B(r) \exp(j 2\pi \mathbf{b}.\mathbf{r})\, d\Omega, \qquad \ldots(1)$$

where **b** is the baseline vector connecting two antennas and **r** is the vector indicating the direction of an element $d\Omega$, within the primary beam (Figure 1). It is possible to explicitly express equation (1) in a Cartesian coordinate system where the baseline vector **b**, as seen from the source, has components u, v, w in the east-west (EW), north-south (NS), and along the direction to the field centre respectively. In that case, the measured visibility is

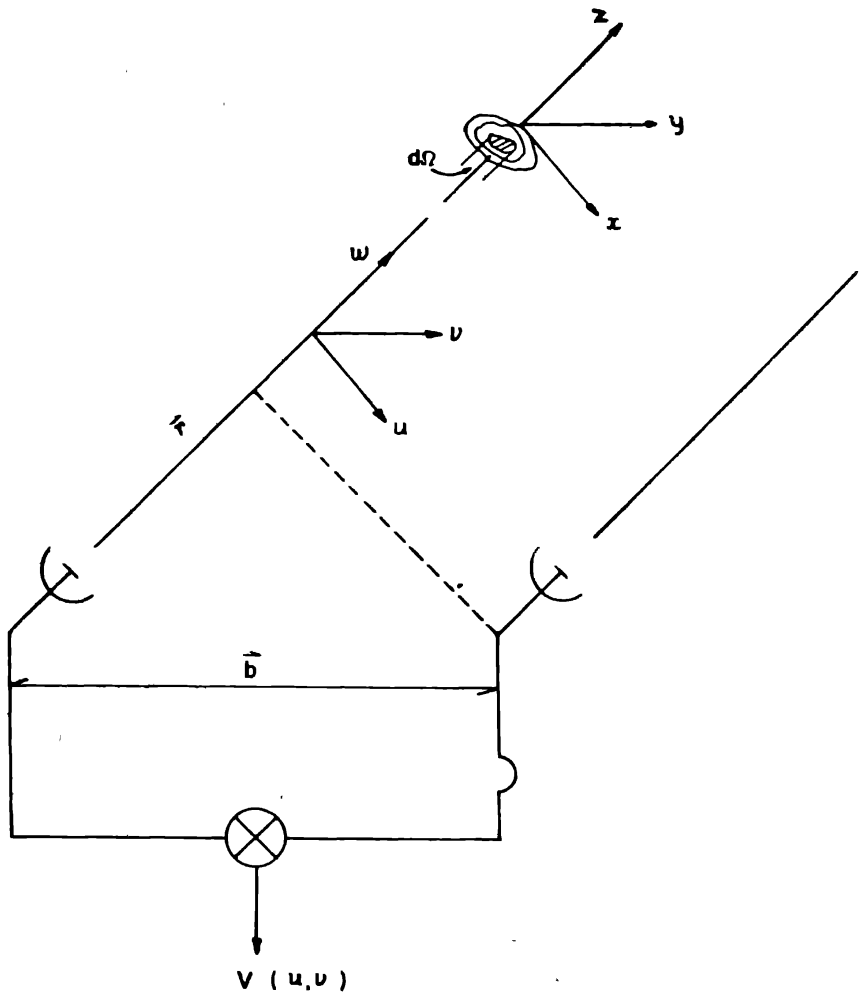

Figure 1. Geometry of interferometer baseline with respect to the sources indicating the coordinate systems (x, y, z) and (u, v, w).

$$V(u, v, w) = \iint B(x, y)\,(1 - x^2 - y^2)^{-1/2} \exp\,[\,j\,2\pi(ux + vy + (\sqrt{(1 - x^2 - y^2)} - 1)\,w)]\,dx\,dy, \quad \ldots(2)$$

where x, y represent the sky coordinates in the east-west and north-south directions respectively. The components u, v, w are also termed as spatial frequencies. When x, y are small i.e. for radio sources having small angular extent) the phase resulting from the term $(\sqrt{(1 - x^2 - y^2)} - 1)\,w$ is neglected and the visibilities can be expressed as

$$V(u, v) = \iint B(x, y) \exp\,[j\,2\pi(ux + vy)]\,dx\,dy. \quad \ldots(3)$$

Thus for small fields of view, the brightness distribution can be derived from the measured visibility function by an inverse Fourier transformation.

As mentioned earlier, the visibility $V(u, v)$ can be measured simultaneously at various spatial frequencies (u, v) if we have several antennas separated by different spacings between them. But this is not an economically viable proposition since it requires a large number of antennas to cover all the necessary spatial frequencies. Alternatively, the earth rotation aperture synthesis in which the radio source is simultaneously tracked from eastern to western horizon by a relatively small number of antennas can be used to measure the complex visibility at a fairly wide range of spatial frequencies (*e.g.* Fomalont & Wright 1974). For a given antenna pair, as the earth rotates, the projected spacing, as seen by the source, changes continuously along an elliptical track in the spatial frequency (u, v) plane with the major axis equal to twice the east-west spacing between antennas and with eccentricity of cos δ where δ is the declination of the source. In order to produce good quality radio maps, it is imperative to have sufficient coverage in the spatial frequency domain and the array configuration of any synthesis radio telescope should conform to this requirement. The map obtained by Fourier transforming the visibilities obtained using all possible baselines in the array has an angular resolution corresponding to the longest baseline between the antennas. In other words, it is equivalent to that obtained by a single large antenna with aperture of the maximum size of the array.

3. Array configuration of OSRT

The design of OSRT is based upon the principle of earth rotation aperture synthesis. It consists of : (a) the Ooty radio telescope (ORT) being divided into 5 sections, and (b) eight antennas of size 23m × 9m.

The ORT is a parabolic cylinder 530m long in the NS and 30m wide in the EW, equatorially mounted with its axis of rotation parallel to the axis of the earth (Swarup *et al.* 1971). While the steering in EW direction is done mechanically, steering in the NS direction within about $\pm$ 45° in declination is achieved by phasing the dipole array along the focal line. The dipole array is divided into 22 modules (each 23m long) having 48 dipoles each (Joshi *et al.* 1988). Normally the 22 modules are combined with proper phasing to form a single telescope which has a narrow voltage response pattern with half width 8 arcmin in the north-south

direction. Since the ORT is the largest element in OSRT, the field of view of OSRT is determined by the voltage pattern of ORT. In order to achieve a large field of view for OSRT in the NS direction, the ORT has been divided into five sections (designated as OA, OB, OC, OD, and OE) and these sections are treated as separate elements of OSRT. Each section consists of four modules of ORT and hence only 20 modules of ORT, excluding the northern and southernmost modules are used for OSRT. This enables us to have a field of view of about 3°.0 × 0°.7 in the EW and NS directions respectively. If needed, still larger field of view in NS (up to 2°) can be obtained by using fewer modules (1 to 4) in each of the five ORT sections. The eight smaller antennas 23m × 9m are also equatorially mounted. As in the case of ORT, beam is steered in the north south direction by phasing the dipoles; and in the east west, mechanically. The distribution of these antennas around ORT has been chosen for maximum possible u, v coverage considering the contraints of the hilly terrain. The location of the OSRT antennas is shown in figure 2. The antenna parameters are summarized in table 2. The hour angle (HA) coverage of OSRT is determined by ORT steerability, which is restricted to — 4h 07m to + 5h 26m. The antenna ECYL closest to ORT can be used from —4h 07m to 00h 00m in HA as it is shadowed by ORT.

The u, v coverages for sources at various declinations and the corresponding synthesized beams (point source response in the synthesized map) are shown in figure 3. The u, v coverages shown are from actual observations. For a wider

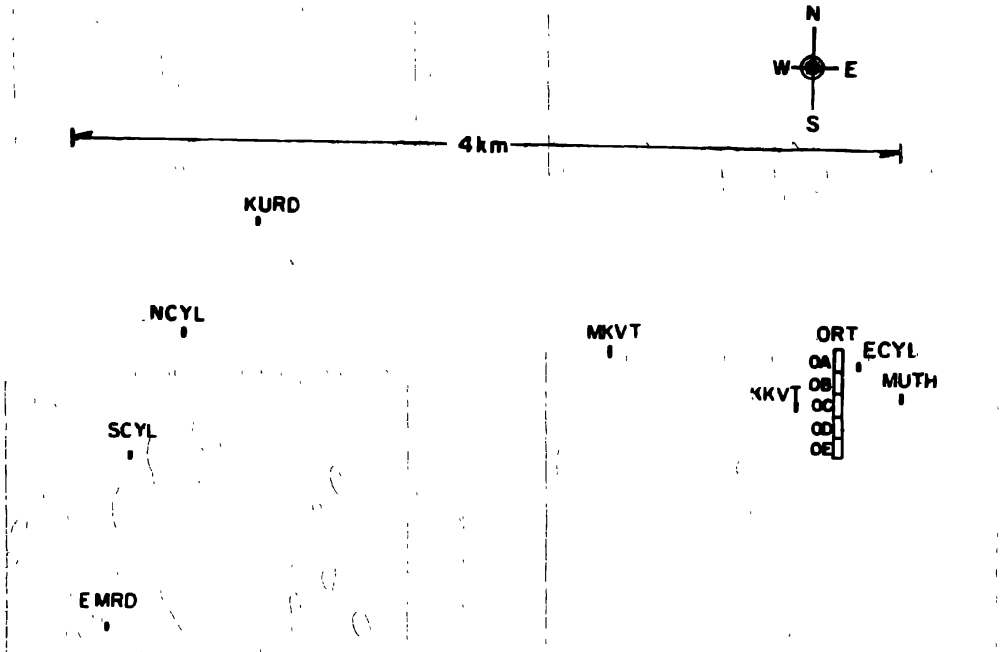

Figure 2. Location of OSRT antennas. ORT is divided into five sections, OA, OB, OC, OD, and OE each of size 92m × 30m. All other antennas are small cylinders of size 23m × 9m. All antennas are parabolic cylinders equatorially mounted with their axes parallel to that of earth's rotation. E-W steering is by phasing the dipole array along the focal line.

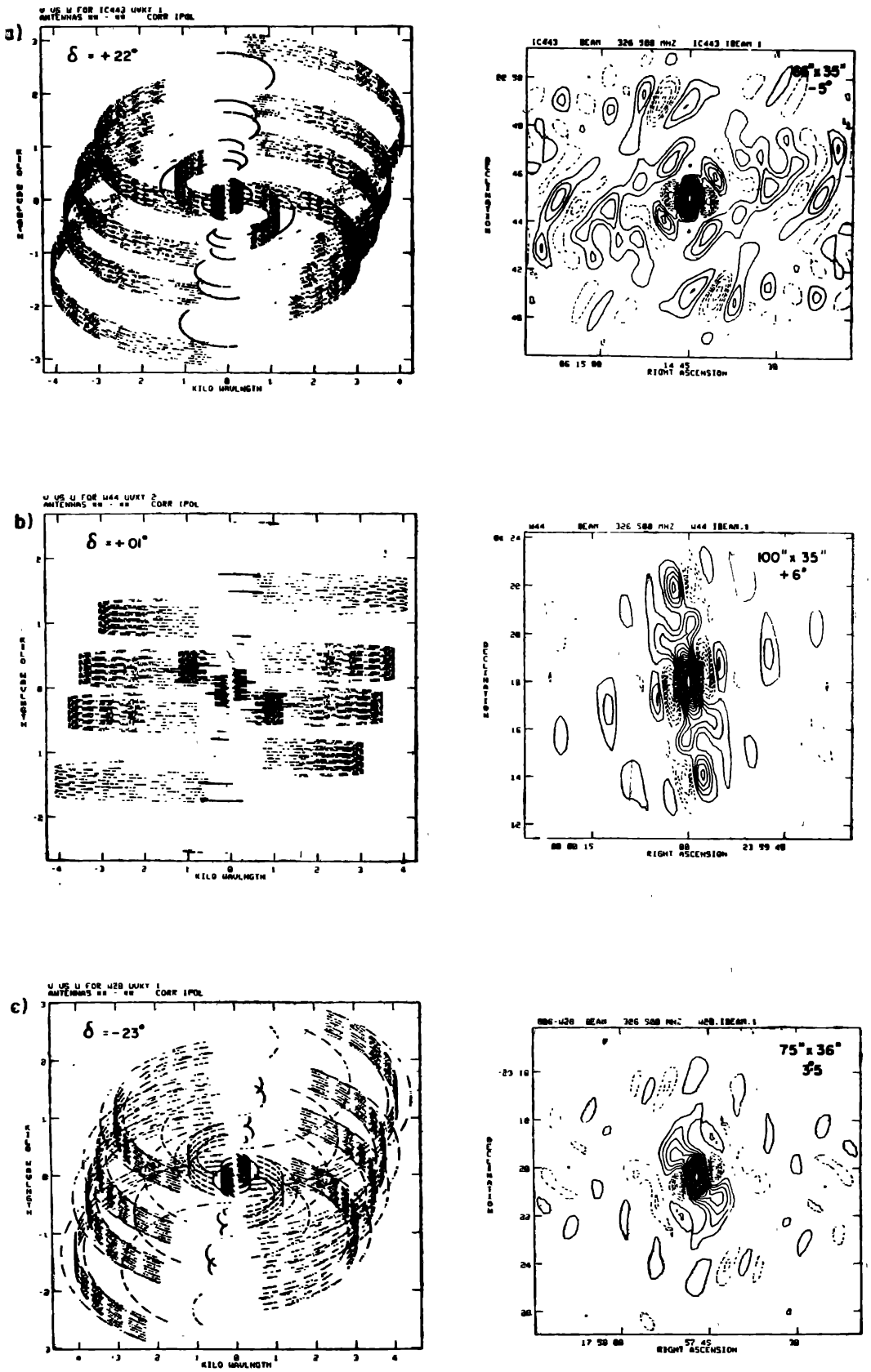

Figure 3. *u*, *v* coverage (left) and synthesized beam (right) of OSRT at declinations (a) + 22°, (b) +01°, and (c) −23°. The size of the synthesized beams and position angle of the major axes are indicated. First contour and contour interval are 5% of peak.

Table 2. Parameters of OSRT

1. Antennas	:	5 ORT sections	30m × 92m
		8 small cylinders	9m × 23m
2. Array size	:	4.2 km east-west	
		2.1 km north-south	
3. Sky coverage	:	− 4h 07m to +5h 30m in HA	
4. Operating frequency	:	327 MHz	
5. Bandwidth	:	3.5 MHz	
6. Field of view	:	2°.8 × 0°.7 (for ORT section with small cylinders)	
7. Resolution	:	35″ × 60″ at $\delta = \pm 30°$	
		35″ × 100″ at $\delta = 0°$	
8. Observable largest structure	:	40′	
9. Sensitivity			
thermal noise	:	5 mJy/beam	for 9 hr integration
confusion noise	:	4 mJy/beam	for 9 hr integration

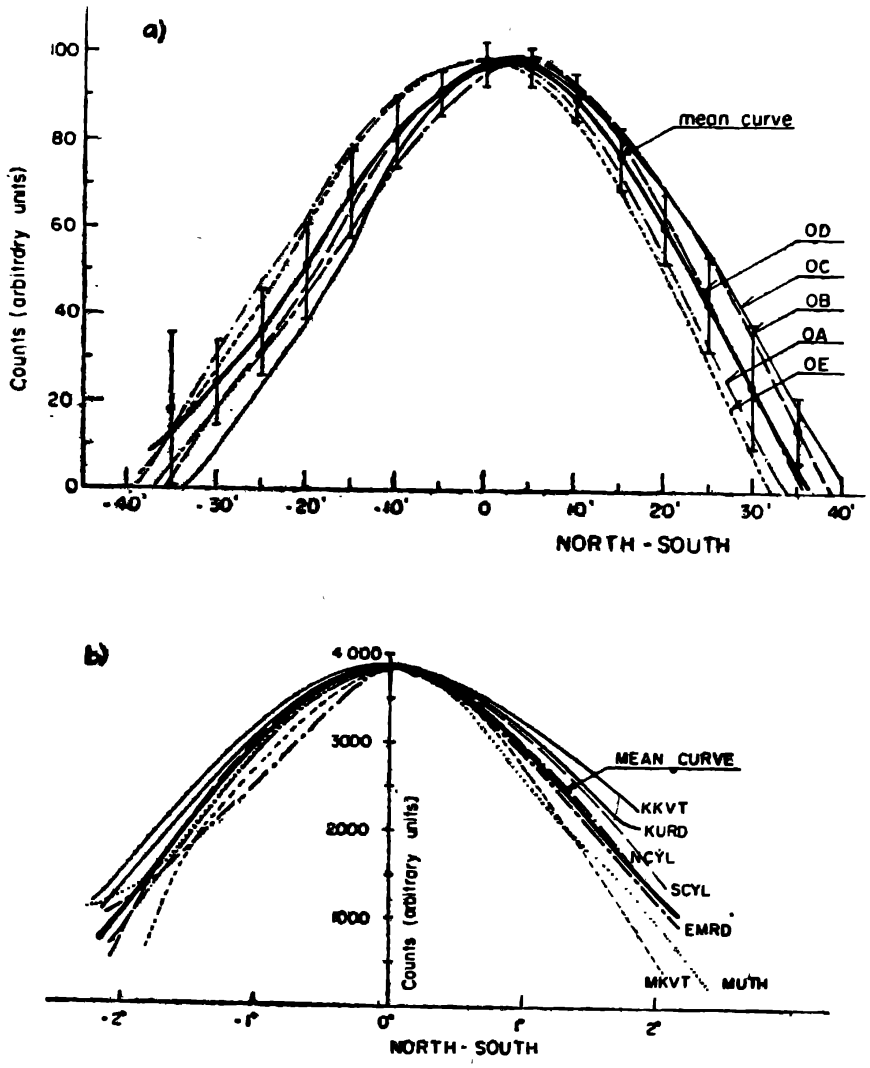

Figure 4. North-south voltage response pattern of the OSRT antennas (a) for selection of ORT, OA, OB, OC, OD, and OE; (b) for the smaller antennas.

field of view, only two modules in each of ORT sections were used, first using the northern two modules in each section and repeating the observations using the

southern two modules. The coverage, though incomplete, is reasonably good at almost all declinations within the range of OSRT. The synthesized beams have maximum side lobe levels of about 25% due to the incomplete u, v coverage. However, the effect of these sidelobes on the radio maps can be alleviated by special image processing techniques like CLEAN (Hogbom 1974), and maximum entropy method (Nityananda & Narayan 1982).

4. Parameters of OSRT

4.1. Field of view

The field of view of a two element radio interferometer is obtained by multiplying the voltage radiation patterns on the individual antennas. This is simply the power pattern of a single antenna, if the antennas are identical. This is not the case with OSRT since it consists of dissimilar antennas. Among OSRT antennas, the five sections of ORT (OA, OB, OC, OD, and OE) have the largest dimension (30m $\times$ 92m) and hence the field of view is the smallest for baselines formed among these sections. It is slightly larger for baselines involving small cylinders and the ORT sections, and the maximum for the baselines involving small cylinders. For most observations, only the baselines between ORT sections and smaller cylinders are used and for all practical purposes the field of view is determined by the voltage radiation pattern of ORT section. In figure 4 are shown the measured voltage patterns in the NS direction for different ORT sections and small cylinders. These patterns differ by (10–20%) from the theoretically expected sinc pattern due to phase errors along the dipole arrays (Joshi *et al.* 1988). For 0° declination the NS field of view is about 31′ for baselines formed among ORT sections and 40′ for baselines involving small cylinders and ORT sections. Owing to projection effect, the field of view at declination δ is increased by sec δ.

The east-west field of view of OSRT is determined by the voltage pattern of ORT sections in the EW direction as they have the largest EW dimensions (30m). The measured EW voltage radiation pattern of ORT is given in figure 5. It was obtained by observing 3C286 using OSRT with ORT pointed at a fixed HA but small cylinders tracking the source. Since most of the observations use only the baselines involving ORT sections and small cylinders, the field of view of OSRT can be taken as $2^\circ.6 \times 0^\circ.7$ sec δ, where δ is the declination of field centre. However, it should be mentioned that the EW field of view can be further limited by the decorrelation suffered due to uncompensated delays for sources away from the phase centre of the observing field. When some of the modules in the ORT sections are switched off, the north-south field of view is broadened correspondingly. For example the north south field of view can be doubled by switching off 2 modules in each ORT section.

4.2. Resolution and large scale structures

The synthesized beam width is inversely proportional to the highest spatial frequency at which the complex visibility has been measured. While the highest

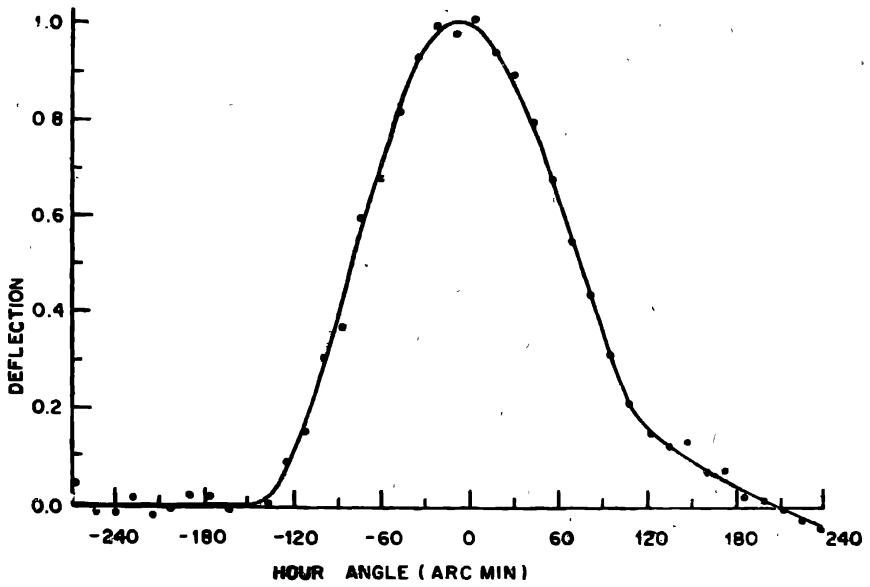

Figure 5. East-west voltage response pattern of ORT which is practically the E-W field of view of OSRT.

spatial frequency component in the east-west direction, u_{max}, depends only on the length of east-west baseline, the highest spatial frequency component in the north-south direction, v_{max}, depends upon length and orientation of the baseline and declination of the source. Though the angular sizes of the synthesized beam in EW and NS directions are proportional to u_{max}^{-1} and v_{max}^{-1} respectively, the exact values are determined by the tapering applied to the observed visibility amplitudes at the highest spatial frequencies. Tapering results in a lower resolution than the theoretically possible values but gives a smoother synthesized beam. Generally, a Gaussian taper is applied so that the highest spatial frequencies have a weight of about 0.25 compared to 1.0 at short spacings. In figure 3 are shown the u, v coverage and synthesized beam of OSRT for three declinations. The corresponding synthesized beam widths for OSRT are listed in table 2 for various declinations.

The sensitivity of a systhesis radio telescope to large scale structures in the sky brighthess distribution depends upon the shortest u, v spacings available and the sampling interval used in the u, v plane. Even though the primary field of view may be large, we may not detect any large scale feature of comparable size if the appropriate sampling at low spacings is not available. The radio interferometer is insensitive to features having angular sizes larger than $\theta \left(u_{min}^2 + v_{min}^2 \right)^{-1/2}$ rad where u_{min} and v_{min} are the minimum spatial frequency components in the EW and NS directions respectively. As in the case of largest u, v spacings, the shortest spacings also depend upon the declination of the source. Even in a synthesis telescope having movable antennas, the shortest spacing is limited to the closest separation i.e. the antenna size itself. For OSRT, which does not have any movable antenna the shortest spacings are provided by baselines formed between

ORT sections and the small cylinder ECYL located 0.08 km east of ORT and KKVT 0.2 km to the west of ORT. Because of cross talk between antennas in OSRT, the shortest spacing that can be reliably sampled is about 80λ to 100λ. Typically the large scale structures observable with OSRT is $< 40'$.

4.3. Sensitivity and confusion limits

For an interferometer pair having an effective area of A in m² and receiving signals over rectangular passband of width, Δf in Hz, the rms noise ΔB (flux density/beam) is given by

$$B = \frac{\sqrt{2}\, kT_{\rm sys}}{\eta_{\rm c}\, A\, \sqrt{\Delta f.t}}, \qquad \ldots(4)$$

where k is the Boltzmann's constant, $\eta_{\rm c}(< 1)$ is the efficiency factor of the digital correlator compared to an analog correlator and t is the integration period in seconds (Napier *et al.* 1983). A synthesis array measures each point in the field of view with sensitivity ΔB given by equation (4). The factor $\sqrt{2}$ appears since the feed systems of the OSRT antennas measure only the NS polarization. The system temperature $T_{\rm sys}$ is contributed by the background sky temperature, losses in the transmission lines and the noise temperature of the front-end amplifier. Assuming that receivers of all OSRT antennas have equal system temperature $T_{\rm sys}$, rectangular passbands of width Δf and that uniform weighting has been used to the visibility data at all spatial frequencies, we can rewrite equation (4) as

$$B = \frac{\sqrt{2}\, kT_{\rm sys}}{\sqrt{\left(\sum_{i=1}^{3} n_{\rm l}\, A_i^2\right) \Delta f.t}}, \qquad \ldots(5)$$

where $n_{\rm l}$ is the number of pairs having effective area $A_{\rm l}$, which is given by the geometric mean of the antenna elements. We have three kinds of antenna pairs in OSRT, namely, (i) pairs formed among ORT sections, (ii) ORT sections with small cylinders, and (iii) among small cylinders. For an observing period of 9 hours, rms noise is about 4.5 mJy per beam. This value differs slightly depending upon the weighting scheme used to the visibility data. Also, in confused regions like the galactic plane, it can be as high as 15 mJy/beam.

4.4. Confusion limit

The sensitivity of a telescope is further limited by confusion. The confusion limit is determined by the distribution of background sources in the sky and the sidelobe levels of the synthesised beam. For an interferometer having two antennas, the rms confusion noise due to background sources is given by (Perley & Erickson 1984)

$$\sigma_{\rm c}^2 = 0.5\, [\int S^2\, n(S)\, dS]\, [\int P^2\, {\rm d}\Omega], \qquad \ldots(6)$$

where P is the power pattern of the individual antennas, $n(S)$ the differential number count, and S the flux density. The second moment of the number count

$\int S^2 n(S)\, dS$ gives the mean square flux density above the mean, and can be evaluated using the log N-log S distribution (*e.g.* Pearson 1975). The beam integral $[\int P^2\, d\Omega]$ for the OSRT is evaluated assuming Gaussian voltage patterns in both EW and NS directions for the ORT and small cylinders. A multi-element interferometer measures the visibility at several independent u, v spacings and the confusion noise is further reduced. Taking all these factors into account, the confusion noise for OSRT for an observing duration of 9 hours is estimated to be $\sim$ 3.7 mJy. This value is broadly consistent with a value of 2 mJy obtained using the criteria of 50 beam-widths (40×60 arcsec^2) per source. We have used for the number density $\sim$ 700,000 and 700,000 sources per steradian above 10 mJy and 1 mJy respectively at 327 MHz, extrapolated from the observations of Windhorst (1984) at 1420 MHz using a spectral index $\alpha = 0.7$ where $S_\nu \sim \nu^{-\alpha}$. It should however be mentioned that the uncertainity in the number density may be larger by a factor of 1.5 (C. R. Subrahmanya, personal communication). Furthermore the confusion noise will depend on the completeness of the u, v coverage. However in the case of OSRT as the system noise is higher at $\sim$ 5–10 mJy/beam, confusion is less important.

5. Special calibration schemes

5.1. Self-calibration

The technique of self-calibration has proven to be very powerful in removing the atmospheric and instrumental errors present in the observed visibility data. (*e.g.* Cornwell 1982). When the errors can be expressed as antenna based (i.e. variations in the complex gains of individual antennas) it is possible to calibrate the antenna gains at any instant using a model for the sky brightness and the observed visibilities at a given instant. In this method the complex gain of individual antennas are corrected such that the visibilities computed by Fourier transforming the model sky brightness reproduce the observed visibilities within the noise level. A preliminary sky brightness obtained from the calibrated visibilities can be used as initial model. The solution to the antenna gains may be improved further iteratively using the successive sky brightness obtained from the visibilities calibrated by the improved antenna gains, as model sky brightness.

Using self-calibration procedure, a dynamic range greater than 600 has been achieved in the OSRT map of Virgo A (Pramesh Rao 1986). On a weak source, NGC 5236, of total flux $\sim$ 5 Jy, a dynamic range of about 50 was attained (Sukumar *et al.* 1987). But the self-calibration procedure is not very useful for weak sources with flux densities less than 5 Jy. In the case of weak sources contribution to the observed visibility from the confusing source within the large primary beam of the small cylinders becomes significant and the errors in the visibility become baseline dependent and hence self-calibration does not yield satisfactory solutions for the antenna gain. For most observations with OSRT particularly in confusing fields like galactic plane only the baselines formed between

ORT sections and small antennas are used and in such cases, it has not been possible to use self calibration.

5.2. *Infield calibration*

As mentioned above it is not always possible to use self-calibration for OSRT observations. However, it is possible to improve the quality of the maps by using a secondary phase calibrator present within the field being mapped. The infield calibration advantageously exploits the NS orientation of ORT to limit the primary beam width in NS direction. In this scheme, the systematic phase errors for individual antennas can be estimated from the visibility data if the mapped region contains a compact source fairly isolated from other sources within the field of view. The five sections of ORT – OA, OB, OC, OD and OE, each 92 m long – are oriented along the north south direction. Thus if one shifts the phase centre to the position of the compact source and adds the visibilities measured by all the ORT sections with any one of the smaller cylinders, the effective primary field of view of ORT is only 8 arcmin instead of 40 arcmin for the individual visibilities measured by OA-small cylinder, etc. The antenna gains are solved using primary calibrator following normal procedure and the visibilities are calibrated. Since ORT sections are part of a phased array, their phases have been assumed to be well calibrated and not varying with time. The calibrated phases of the measured visibility are adjusted for a shift in phase centre corresponding to position of the compact source (infield calibrator) within the field of view. The visibilities of any one of the small cylinders with all five ORT sections are then added. Since this visibility is restricted to a narrow field of view of 8 arcmin in the north south direction, any contamination from neighbouring sources is reduced. Their contribution can be further reduced by averaging the visibilities over a scan ($\sim$ 10–30 min). The resultant phase of the average visibility is treated as the phase error of the particular small cylinder caused by the ionosphere etc. An isolated source above 0.3 Jy can be used as a secondary calibrator. This procedure considerably reduces phase variations arising due to ionosphere for antennas beyond 1 km from ORT. However, for the nearby antennas ($<$ 0.5 km) usually the confusion from the extended emission is very severe and we have to rely only on the primary phase calibrator.

6. Data acquisition and analysis

Two computers are used for OSRT data processing. A PDP 11/24 minicomputer is used to control the antennas, set delays, read and store the outputs of DDLC. All calibration and data processing are done with a PDP 11/70 computer. In figure 6 is shown the overall scheme : scheduling observations, data acquisition, editing, calibration, making maps, cleaning and improving the quality of the maps etc. A brief description is given below.

The data acquisition is done through a program called SCANSKY. It accepts information on the observation schedule from a file containing name and position of the sources to be observed and the sequence of observations. From these data

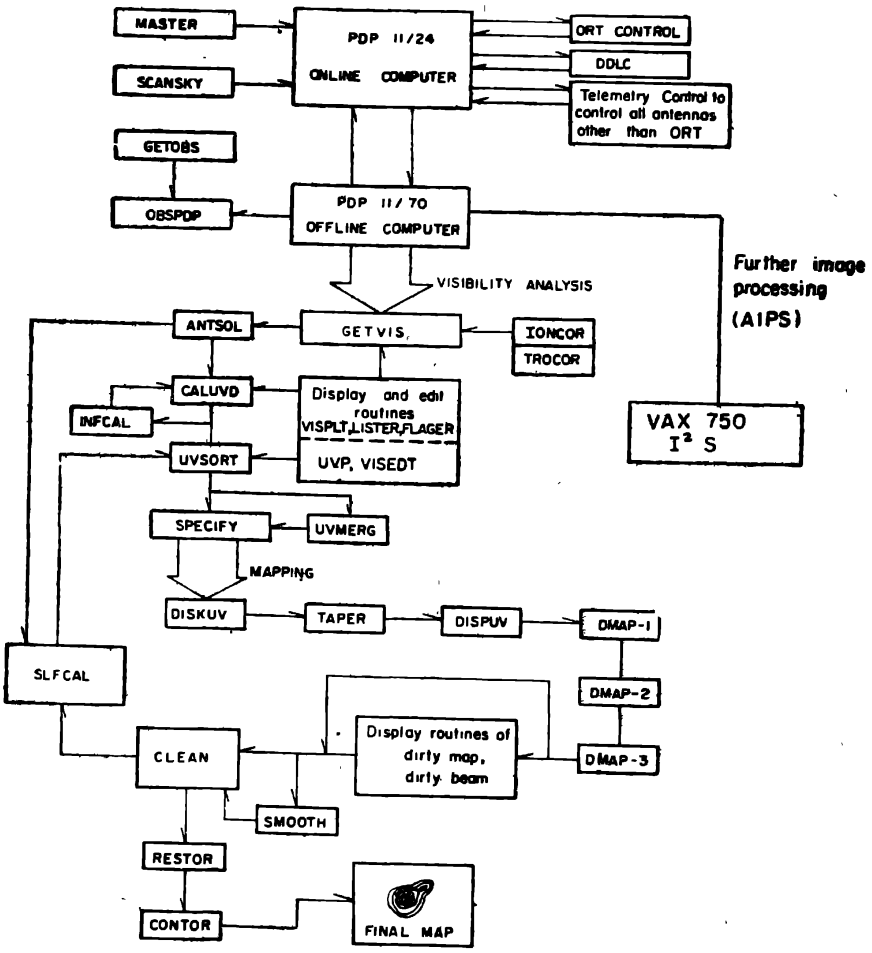

Figure 6. Flow diagram of the OSRT observing and data processing schemes, using PDP 11/24, PDP 11/70, VAX 11/750 computers and I^2S image processing system.

the SCANSKY calculates and sends delays and fringe rates to the DDLC as well as commands to the telemetry for pointing and tracking the antennas. In a given session of observation it is possible to include a number of 'fields', each field pertaining to a given right ascension (RA). A field can have a number of 'sub-fields' each centred at a different declination but at the same RA. Several such fields can be observed in quick succession as rapid switching of declination is possible with the diode phase shifters in the dipole array of the antenna feeds. This provision is best utilised for frequently observing calibration sources. At the end of an integration period (typically 6s) SCANSKY receives from the sine and cosine correlator of the DDLC, the real and imaginary values of the complex visibility for all the baselines, normalizes them using self correlator values and stores them for further analysis.

The post analysis is done in the following sequence : the 6s complex visibilities from a given baseline for a subfield are added to obtain 1 min averages which form the data base. Checks for bad antennas and corrections are made and data

are flagged accordingly. Phase correction to compensate for atmospheric and ionospheric propagation effects is then applied. The Bent model for the ionosphere (Bent *et al.* 1972) and a simple exponential troposphere model over Ooty are used. Predicted values of f_0F_2 and M(3000)F_2 supplied by the National Physical Laboratory, New Delhi, are also used (Laxmi *et al.* 1979). From the visibility data on the calibrating sources, antenna gains, both amplitude and phase for each antenna are derived and then applied to calibrate the data for other sources. At each stage in the above sequence it is possible tc examine the data and flag bad data. The calibrated visibilities are gridded and then Fourier transformed to get 'dirty beams' and 'dirty maps' which are CLEANed to get the final maps. The calibrated visibility obtained form OSRT can be further processed using the standard AIPS package of the National Radio Astronomy Observatory, with the image processing facility at Ooty consisting of VAX 11/750 computer and an International Imaging (I^2S) display.

7. Some OSRT observation

Some of the early results from OSRT have been summarized by Swarup (1984). The operating frequency at 327 MHz is best suited for studying steep spectrum

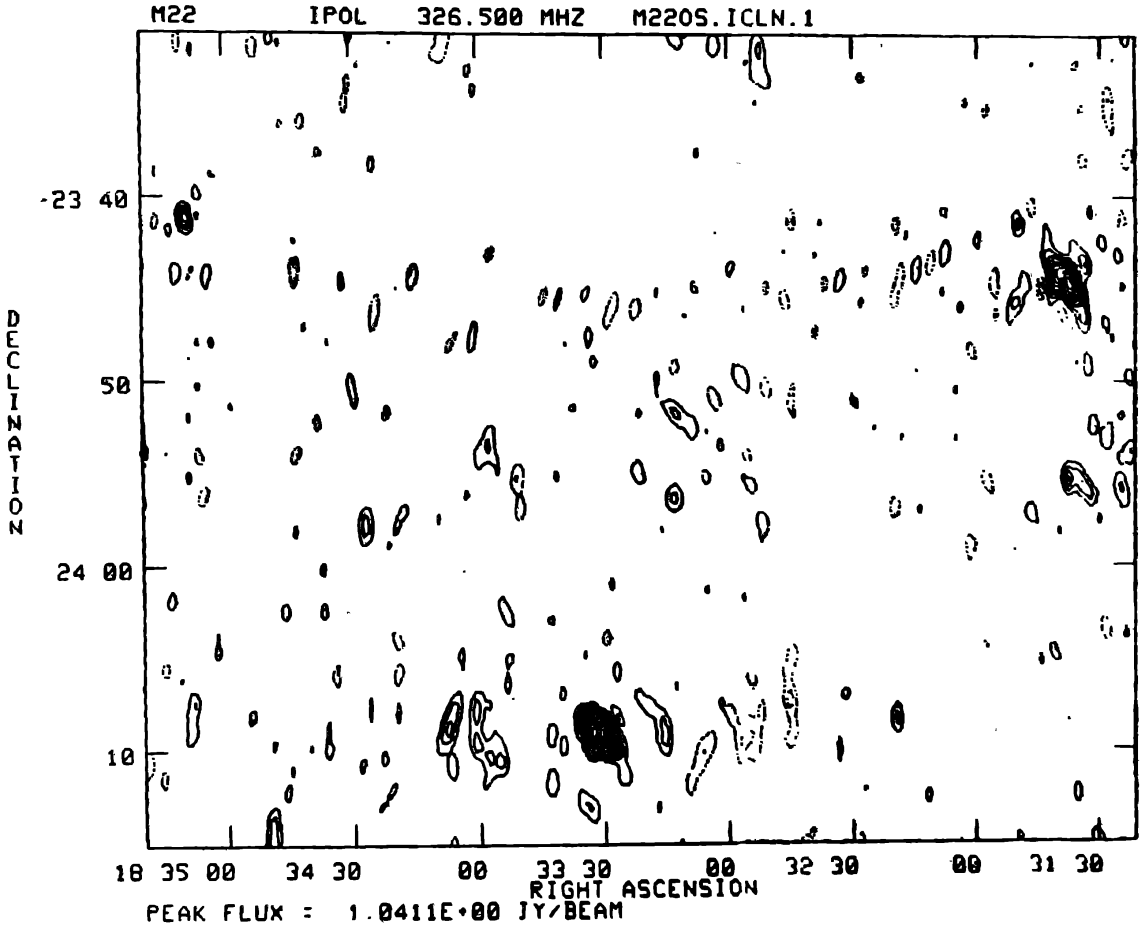

Figure 7. OSRT map of a field around globular cluster M22. The first contour and interval are at 30 mJy/beam. The restoring beam was 70″ × 29″.

radio emission such as halos in galaxies and clusters of galaxies. OSRT is being used mostly for high resolution mapping (*e.g.* Velusamy 1987, Joshi *et al.* 1986). The high sensitivity of OSRT is also used for accurate flux density measurement. OSRT is also being used for monitoring meter wavelength variability in about 170 sources with flux densities > 1 Jy (Ghosh & Pramesh Rao 1987).

OSRT map of the region around the globular cluster M22 is shown in figure 7. The rms noise near the map centre is about 10 mJy. There is no evidence for the presence of any radio source at the known x-ray source position in the cluster. The sources farther away from the map centre particularly one near the western boundary show artefacts due to phase errors introduced by neglecting the w-term in equation (2). For wide field mapping with OSRT one must include the effects of w-term by making mosaic maps using, for example, MX in AIPS.

The radio source Virgo A (M87, 3C274), one of the strongest radio sources in the sky, is known to have an extended diffuse halo around its bright nuclear core. But, the halo has not been well mapped at meter wavelengths because of its low surface brightness and very high brightness of the core. Since the core is strong and only partially resolved at the longest baselines it has been possible to make a self-calibrated map of Virgo A at 327 MHz using the OSRT. In this high dynamic

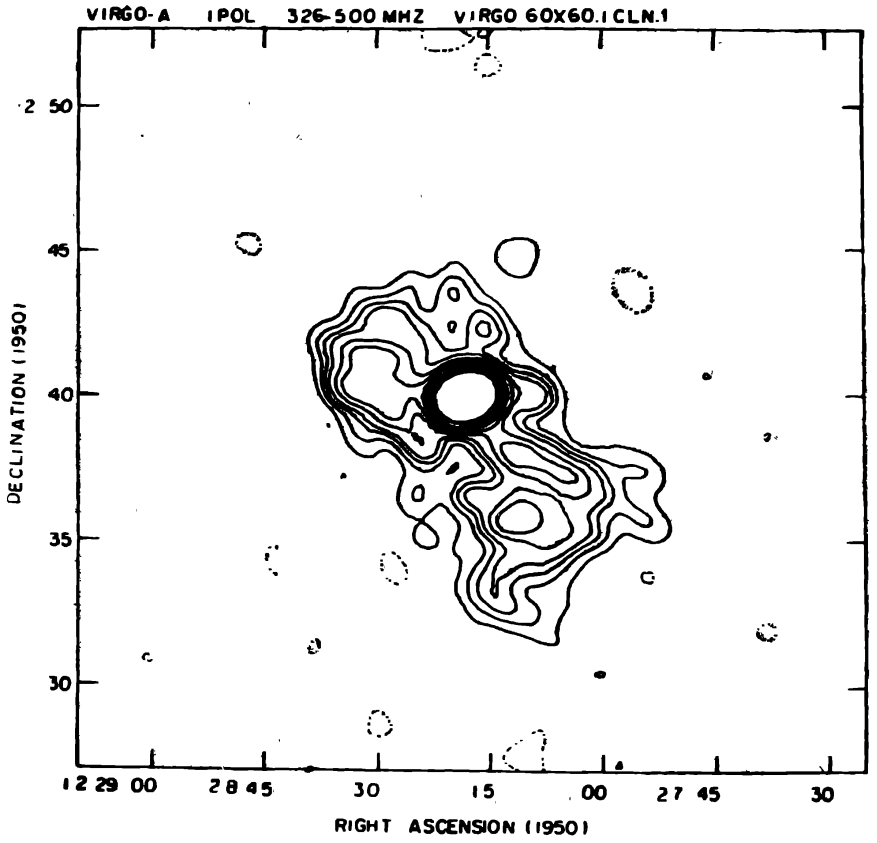

Figure 8. OSRT map of Virgo A. The contour levels are 1, 2, 3, 4, 6, 8, 12, 16, 20, 30, 40 Jy/beam. The restoring beam was $60'' \times 60''$.

range map (figure 8) with a resolution of 1′ the halo is resolved, indicating an S shaped symmetry suggesting its origin due to precessing beam (Pramesh Rao 1986).

The OSRT with its high sensitivity and resolution, large field of view and operation at meter wavelength is well suited for a survey of clusters of galaxies which are known to contain very steep spectrum (VSS) radio sources with spectral indices $\alpha > 1.2$ and head-tail radio galaxies with extended diffuse steep spectrum tails. The VSS sources are remnants of old radio galaxies confined by the hot thermal gas. The head-tail sources owe their morphology to the motion of their parent galaxies through the intracluster medium leaving behind a trail of relativistic electrons which is confined by the hot ICM gas. Such sources can be used as probes to study the dynamics of ICM. A major program has been started for mapping a large number of clusters using the OSRT (Joshi *et al.* 1986). As an example, the map of the cluster A 401 is shown in figure 9. It is seen that the map is dominated by a head-tail source close to the cluster centre.

A survey of the galactic plane at 327 MHz is being carried out with the OSRT. The primary objective of this survey is to search for new supernova remnants

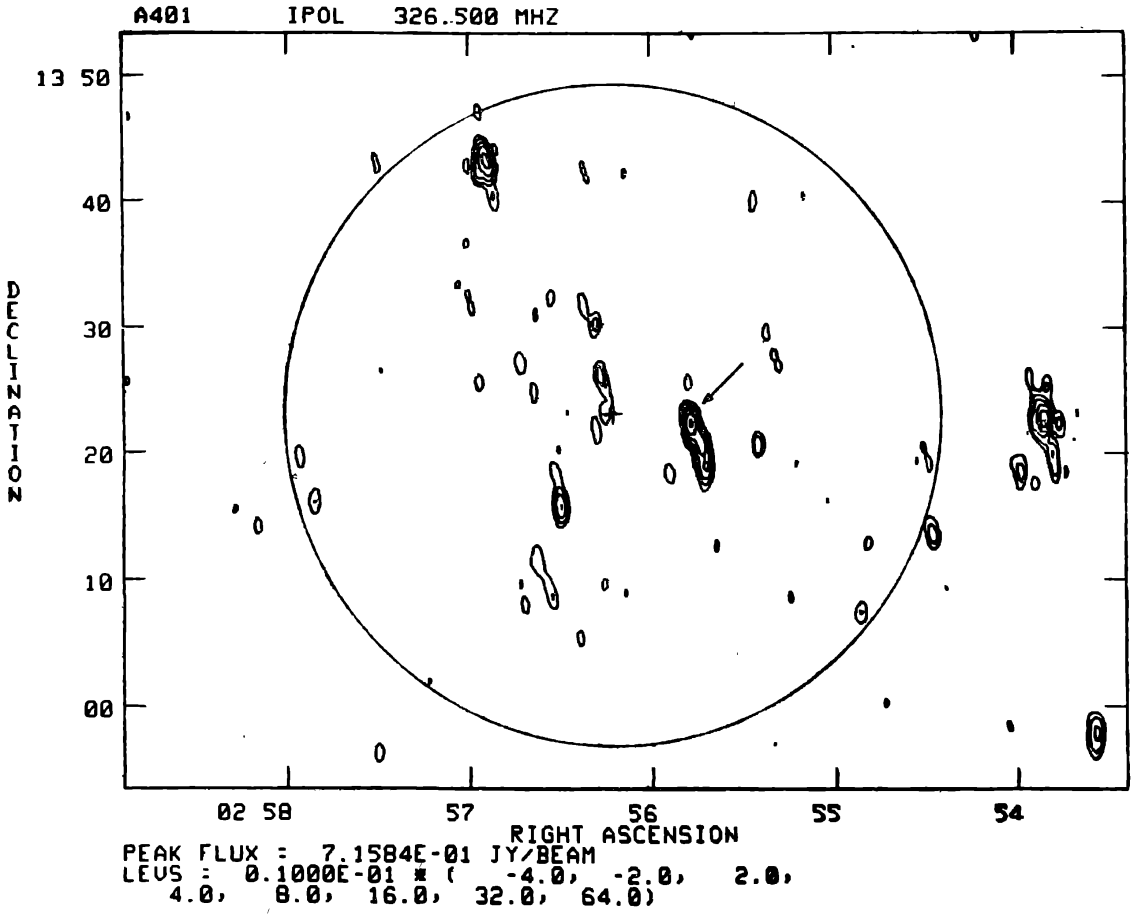

Figure 9. OSRT map of cluster of galaxies Abell 401. The restoring beam was 105″ × 31″. The circle indicates the extent of the optical cluster. The cross marks the centre of the cluster. The arrow indicates the head tail radio source near the centre.

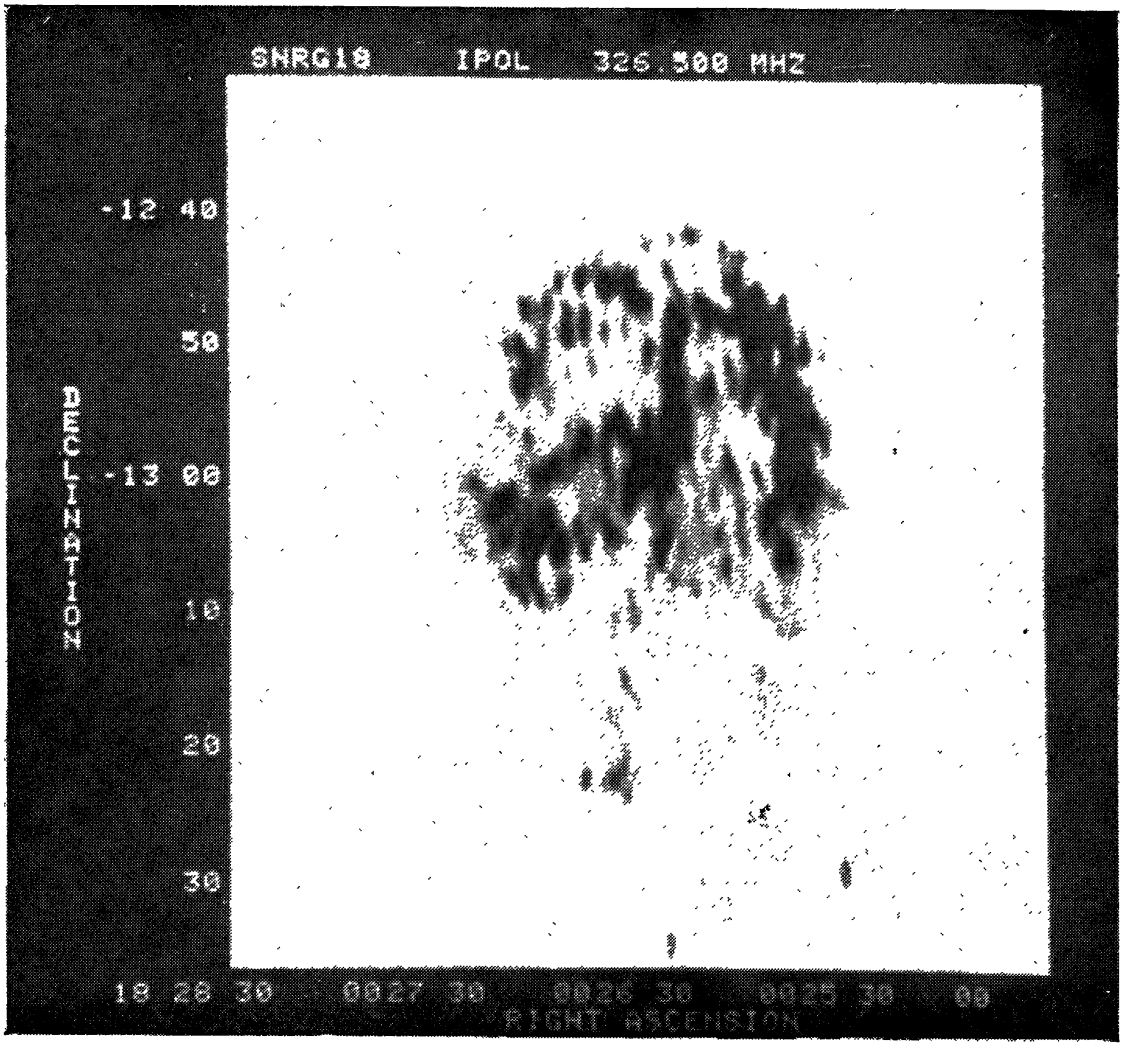

Figure 10. Grey scale image of galactic nonthermal source G18.95-1.1. The restoring beam was 96″ × 36″. The OSRT map shows supernova remnant shell surrounding a central object.

(SNRs) in the three distinct classes, namely (a) shell, (b) Crab-like pulsar driven synchrotron nebulae, and (c) Crab-like nebulae surrounded by shells. About 50 fields of 3° × 0°.7 along the galactic plane have been observed (Velusamy 1987). In figure 10 is shown OSRT map G 18.95–1.1, which was identified as shell type remnant with a central object (Patnaik *et al.* 1988). This survey will be useful for identifying more SNRs which would enable a better understanding of the supernovae that result in the formation of shells and pulsar-driven synchrotron nebulae.

Acknowledgements

It is a pleasure to thank Dr V. R. Venugopal for critically reading the manuscript. We thank the staff members of Radio Astronomy Centre, Ootacamund whose

untiring efforts have made OSRT a reality. OSRT was constructed and is being maintained by the Tata Institute of Fundamental Research with the financial support of the department of atomic energy, government of India. The OSRT data were processed at the National Image Processing Facility for Astronomy, Radio Astronomy Centre, Ooty. This facility is financed by the department of science and technology, government of India.

References

Bent, R. B., Llewellyn, S. K. & Schring, P. E. (1972) *Space Res.* **12**, 1208.
Bracewell, R. 1958) *Proc. IRE* **46**, 97.
Cornwell, T. J. (1982) in *Proc. NRAO-VLA Workshop* on Synthesis Mapping (eds : A. R. Thompson & L. R. D'Addario) NRAO.
Fomalont, E. B. & Wright, C. H. (1974) in *Galactic and Extragalactic Radio Astronomy* (eds : G. L. Verschuur & K. I. Kellermann) Springer.
Ghosh, T. & Pramesh Rao, A. (1987) in *Proc. Green Bank Workshop on Large Scale Surveys of Sky* (ed. : J. Lockman & J. J. Condon) NRAO.
Hogbom, J. (1974) *Ap. J. Suppl.* **15**, 417.
Joshi, M. N., Kapahi, V. K. & Bagchi, J. (1986) *Proc. NRAO Workshop on Continuum Radio Processes* in Clusters of Galaxies" (eds : C. P. O'Dea & J. M. Uson) NRAO.
Joshi, M. N., Swarup, G., Bagri, D. S. & Kher, R. K. (1988) *Bull. Astr. Soc. India* **16**, 111.
Laxmi, D. R., Aggarwal, S., Pasricha, P. K. & Reddy, B. M. (1979) *Ind. J. Radio Space Phys.* **8**, 101.
Napier, P. J., Thompson, A. R. & Ekers, R. D. (1983) *Proc. IEEE* **71**, 1295.
Narayana, D. L., Venkatasubramanian, T. L. & Bagri, D. S. (1988) *Bull. Astr. Soc. India* (submitted).
Nityananda, R. & Narayan, R. (1982) *J. Ap. Astr.* **3**, 419.
Patnaik, A. R., Velusamy, T. & Venugopal, V. R. (1988) *Nature* **332**, 136.
Pearson, T. J. (1975) *Mon. Not. R. astr. Soc.* **171**, 475.
Perley, R. A. & Erickson, W. C. (1984) *VLA Scientific Memorandum No.* 146.
Pramesh Rao, A. (1986) *Proc. NRAO Workshop on Continuum Radio Processes in Clusters of Galaxies* (eds : C. P. O'Dea & J. M. Uson) NRAO.
Ryle, M. (1962) *Nature* **194**, 517.
Sankararaman, M. R., Subramanian, N., Balasubramaniam, R. (1982) *J. I. E. T. E.* **28**, 216.
Sukumar, S., Kelvin, V. & Grave, R. (1987) *Astr. Ap.* **184**, 71.
Swarup, G. *et al.* (1971) *Nature Phys. Sci.* **230**, 185.
Swarup, G. (1984) *J. Ap. Astr.* **5**, 139.
Swenson, G. W. & Mathur, N. C. (1968) *Proc. IEEE* **56**, 2114.
Velusamy, T. (1987) in *Proc. Green Bank Workshop on Large Scale Surveys of Sky* (eds : F. J. Lockman & J. J. Condon) NARO.
Windhorst, R. A. (1984) Ph.D. Thesis, Univ. of Leiden.